ELSEVIER

Journal of Hepatology 50 (2009) 766–778

Journal of Hepatology

www.elsevier.com/locate/jhep

miR-15b and miR-16 are implicated in activation of the rat hepatic stellate cell: An essential role for apoptosis☆

Can-Jie Guo, Qin Pan*, Ding-Guo Li*, Hua Sun, Bo-Wei Liu

Digestive Disease Laboratory and Department of Gastroenterology, School of Medicine, Shanghai Jiaotong University, Xinhua Hospital, No. 1665 Kongjiang Road, Shanghai 200092, China

***Background/Aims*: To reveal the microRNA (miRNA) expression profile and related roles in rat HSCs during activation.**

***Methods*: miRNA expression profiling was analyzed in quiescent and in culture-activated HSCs by microarray. The differentially expressed miRNAs, as verified by RT-PCR, were subjected to gene ontology (GO) analysis. Furthermore, the effects of miR-16 and miR-15b on the apoptosis of activated HSCs were investigated by Hoechst 33258, TUNEL staining and annexin-V/PI labeling flow cytometry. The underlying mechanism related to Bcl-2 and caspases was assessed.**

***Results*: The upregulated and downregulated miRNAs in activated HSCs were 12 miRNAs and 9 miRNAs, respectively. The differential expression of miR-16, -15b, -122, -138, -143, and -140 was validated. High-enrichment GOs containing apoptosis-related targeted genes and miRNA–gene networks characterized by Bcl-2, which was targeted by the miR-15/16 family, uncovered the critical role of miR-16 and miR-15b in apoptosis. Restoring the intracellular miRNAs by miR-16 and miR-15b administration greatly reduced Bcl-2, and increased the expression of caspases 3, 8, and 9. Significantly elevated rates of apoptosis were then induced in activated HSCs.**

***Conclusions*: The activation of HSCs relate to 21 miRNAs. Among these, mir-15b and miR-16 may be essential for apoptosis by targeting Bcl-2 and the caspase signaling pathway.**

***Keywords*: Hepatic stellate cells; Activation; miR-16; miR-15b; Gene ontology; Bcl-2; Caspase; Apoptosis**

1. Introduction

Liver fibrosis, which is characterized by excessive accumulation of extracellular matrix (ECM) and distortion of lobular structure, is the common outcome of most types of chronic liver disease. Although many types of hepatic cells, including hepatocytes, cholangiocytes, Kupffer cells and so on, have been shown to be involved in fibrogenesis, hepatic stellate cells (HSCs) are generally considered to be the major ECM producer responsible for liver fibrosis [1]. Resting HSCs usually locate in the perisinusoidal space with vitamin A-containing lipid droplets. However, their morphology and physiology alter dramatically during myofibroblastic transdifferentiation, also known as activation, which serves as the critical step in the initiation as well as progression of liver fibrosis [2,3]. The most important phenotypic alterations of activated HSCs, as defined by theirs actions in liver fibrogenesis, lie in the active proliferation, autocrine and/or paracrine fibrogenetic factors, inordinate ECM synthesis and secretion, and resistance to apoptosis, etc.

Received 24 July 2008; received in revised form 28 October 2008; accepted 6 November 2008; available online 2 February 2009

Associate Editor: C. Trautwein

☆ The authors declare that they do not have anything to disclose regarding funding from industries or conflict of interest with respect to this paper.

* Corresponding authors. Tel./fax: +86 21 62712237.

E-mail addresses: lidingguo13612@yahoo.com.cn (D.-G. Li), pan_qin@yeah.net (Q. Pan).

Abbreviations: miRNA, microRNA; HSC, hepatic stellate cell; GO, gene ontology; ECM, extracellular matrix; 3′ UTR, 3′ untranslated region; ALB, albumin; CK-19, cytokeratin-19; FDR, false discovery rate; SD, standard deviation.

0168-8278/$36.00
doi:10.1016/j.jhep.2008.11.025

Recent studies attempt to reveal the mechanism underlying HSCs activation. As a result, hundreds of genes relevant to various functions have been reported to play a role in the process [4]. However, a full understanding of HSCs activation is still beyond our reach because of its complexity, especially the intricate regulation of gene expression. Fortunately, identification of multiple miRNAs along with a comprehensive description of the miRNA/mRNA interaction network may add a new level to our knowledge of the gene regulation throughout HSCs activation.

The miRNAs are a number of small non-coding RNAs of 21–25nt, which usually negatively modulate gene expression at the post-transcriptional level by incomplete or complete complementary binding to target sequences within the 3′ untranslated region (3′UTR) of mRNA [5]. They have been identified in most kinds of cells and tissues. It is currently estimated that 10-30% of genes, especially the members of signal transduction networks, may be regulated by miRNAs. Moreover, there is an accumulating body of evidence that miRNAs are implicated in a variety of biological processes, such as cell proliferation, differentiation, apoptosis, tumorigenesis, etc [6]. Aberrant and/or absent expression of miRNA is often associated with pathophysiological disorders [7–9]. Therefore, the activation of HSCs, a liver-specific disorder presenting abnormal biological processes, is likely to be regulated by miRNAs.

Given the potential role of miRNAs, their expression was profiled in quiescent and spontaneously activated rat HSCs by microarray. The differentially expressed miRNAs were then selected, validated and subjected to GO analysis. The miRNAs and target genes predominating in the miRNA–gene regulatory networks were further investigated in HSCs in an attempt to provide new insight into the limited understanding biological process of HSCs activation.

2. Materials and methods

2.1. Isolation, culture, and identification of rat HSC

Primary HSCs were isolated from three normal male Sprague–Dawley rats (Shanghai Laboratory Animal Center of Chinese Academy of Sciences, weighting 400–500 g) by *in situ* perfusion and density-gradient centrifugation [10]. The rats received humane care according to the Guide for the Care and Use of Laboratory Animals of the Chinese Academy of Sciences. All the materials for HSCs isolation were obtained from commercial sources as previously described [11].

The isolated HSCs were cultured in DMEM, supplemented with 10% FBS, 100 U/ml penicillin, 100 mg/ml streptomycin, and 2 mmol/l glutamine. Thereafter, the quiescent and totally activated HSCs were harvested at day 2 and day 14, respectively. Their purity was detected by Oil red O staining for lipid droplets, and QRT-PCR for desmin, albumin (ALB), CD31, CD68, and cytokeratin-19 (CK-19). Detailedly, total cellular RNA, being extracted from HSCs at day 2 and day 14 using Trizol reagent (Invitrogen, Carlsbad, CA, USA), was subjected to RT reaction by ExScript RT reagent kit (TAKARA, Kusatsu, Japan) and Real-time PCR by SYBR Premix Ex Taq (TAKARA, Kusatsu, Japan) on a LightCycler (Roche Diagnostics GmbH, Penzberg, Germany). Primer sequences for these biomarkers were exhibited in Table 1. Furthermore, the phenotype of HSCs was evaluated by immunocytochemistery using monoclonal antibodies specific for desmin and α-SMA (Sigma–Aldrich, St. Louis, MO, USA) (1:100) [12], and also by QRT-PCR for desmin and α-SMA as mentioned above.

2.2. LNA-based miRNA microarray analysis

Purified RNA was labeled with a miRCURY Hy3/Hy5 labeling kit (Exiqon, Vedbæk, Denmark). The Hy3™-labeled samples and Hy5™-labeled reference pool RNA samples were then mixed pair-wise and hybridized to the miRCURY LNA array version 8.0 (Exiqon, Vedbæk, Denmark). The hybridization was performed according to the miRCURY LNA array manual. Following hybridization, the slides were washed by Wash buffer kit (Exiqon, Vedbæk, Denmark), dried and scanned on a GenePix 4000B array scanner (Molecular Devices Co., Sunnyvale, CA, USA). The results were subjected to unsupervised hierarchical clustering (Cluster 3.0) and TreeView analysis (Stanford University, Standford, CA, USA).

2.3. QRT-PCR of miRNA

Differentially expressed miRNAs of miR-16, miR-15b, miR-122, miR-138, miR-143, and miR-140 were selected at random for verification. Expression of these mature miRNAs was assayed using stem–loop RT followed by PCR analysis as previously described [13]. PCR was performed in triplicate for each sample. The relative amount of miRNAs was normalized against U6 snRNA, and the fold change for each miRNA was calculated by the 2-[delta][delta] Ct method [14]. The primers used for stem–loop RT-PCR are shown in Table 2.

2.4. Gene ontology (GO) analysis

GO analysis was applied in order to organize genes into hierarchical categories and uncover the miR-Gene Regulatory Network on the basis of biological process and molecular function [15]. In detail, two-side Fisher's exact test and $\chi 2$ test were used to classify the GO category, and the false discovery rate (FDR) was calculated to correct the *P*-value. We chose only GOs that had a *P*-value of <0.001 and a FDR of <0.05. Within the significant category, the enrichment Re was given by:

$$\mathrm{Re} = (n_f/n)/(N_f)/N)$$

where n_f is the number of flagged genes within the particular category, n is the total number of genes within the same category, N_f is the number of flagged genes in the entire microarray, and N is the total number of genes in the microarray. Afterwards, the apoptosis-related network of miRNA–mRNA interaction, representing the critical miRNAs and their targets, was established according to the miRNA degree.

2.5. Treatment of activated HSCs by miR-16 and miR-15b

Activated HSCs were cultured at a density of 2×10^7 ml^{-1} in 75 cm^2 uncoated plastic plates and divided into normal group, negative control group, miR-15b-treated groups (50, 100, and 150 nM miR-15b), and miR-16 treated groups (50, 100, and 150 nM miR-16). Thereafter, the activated HSCs were transfected by mimics of miR-15b or miR-16, which were designed as described [16] (Table 3) and synthesized by Dharmacon Research, Inc. (Lafayette, CO, USA), for 6 h using Lipofectamine 2000 (Invitrogen, Carlsbad, CA, USA). All experiments were repeated in triplicate.

2.6. Detection of Bcl-2 by semiquantitative RT-PCR, qRT-PCR, and Western blot

RNAs were extracted as previously described, and RT reactions were performed with total RNA (2 μg) according to ReverTra Ace kit (Toyobo, Osaka, Japan). The product was amplified in a reaction

Table 1
Primers used in qRT-PCR.

Gene	Annealing temperature (°C)	Accession No.	Product size (bp)	Number gene primer (5′ → 3′)
alpha-SMA	55	NM-031004	78	F:5′-CGA AGC GCA GAG CAA GAG A-3′ R:5′-CAT GTC GTC CCA GTT GGT GAT-3′
Desmin	52	NM-022531	245	F:5′-CTT CAG GAA CAG CAG GTC-3′ R:5′-ATC TCG CAG GTG TAG GAC-3′
ALB	56	NM-134326	321	F:5′-GAC TGC CCT GTG TGG AAG AC-3′ R:5′-CGA AGT CAC CCA TCA CCG TC-3′
CD68	56	NM-001031638	62	F:5′-TCATGGGAATGCCACAGTTTC-3′ R:5′-GAGGGCCAACAGTGGAGAA-3′
CK19	56	NM-199498	388	F:5′-CACTACGCAGATCCAGATAAACA-3′ R:5′-GAAGTCGCACTGGTAGCAAG-3′
CD31	56	U77697	360	F:5′-CTT CAC CAT CCA GAA GGA AGA GAC-3′ R:5′-CAC TGG TAT TCC ATG TCT CTG GTG-3′
Bcl-2	62	NM-016993	116	F:5′-TGAACCGGCATCTGCACAC-3′ R:5′-CGTCTTCAGAGACAGCCAGGAG-3′
GAPDH	62	NM-002046	450	F:5′-ACCACAGTCCATGCCATCAC-3′ R:5′-TCCACCACCCTGTTGCTGTA-3′

F, forward primer; R, reverse primer.

volume of 25 μl including 2 μl RT products, 1× reaction buffer, 1 U Ex Taq DNA polymerase (TaKaRa, Japan) and 20 pmol of each primer. PCRs were performed for 20 cycles at 94 °C for 45 s, 60 °C for 30 s, 72 °C for 30 s. Primer sequences were listed in Table 1. qRT-PCR was done as mentioned above.

Total proteins were prepared by standard procedures and quantified by the BCA method (Pierce, Rockford, USA). Thirty micrograms of protein per sample was loaded onto a 10% SDS-polyacrylamide gel. After electrophoresis, the protein was transferred onto a PVDF membrane (Millipore, Billerica, MA, USA) by electro-elution. The membrane was incubated with anti-Bcl-2 antibody (1:200; Santa Cruz, CA, USA) overnight at 4 °C and HRP-conjugated goat anti-mouse IgG (1:5000; Jackson ImmunoResearch) for 2 h at room temperature. After washing, the membrane was processed using SuperSignal West Pico chemiluminescent substrate (Pierce, Rockford, IL, USA), anti-actin antibody (Santa Cruz, CA, USA) (1:500) as an internal standard.

2.7. Luciferase activity assay

The 3′UTR of rat Bcl-2 cDNA containing the putative target site for miR-15b and miR-16 was amplified by PCR and inserted into the pGL3 control vector (Promega, Madison, WI, USA) immediately downstream from the stop codon of luciferase (pGL3-Bcl2-3′-UTR). A mutant version of the 3′UTR, with a deletion of 6bp (3′M) from the site of perfect complementarity was also generated by the QuikChange II Site-Directed Mutagenesis Kit (Stratagene, La Jolla, CA, USA). For reporter assays, The cells were transiently transfected with wild-type or mutant reporter plasmid and miRNAs (indicated in Fig. 7) using lipofectamine 2000 (Invitrogen, Carlsbad, CA, USA). Firefly and Renilla luciferase activities were measured consecutively by dual-luciferase assays kit (Promega, Madison, WI, USA) 24 h after transfection.

2.8. Apoptosis assay

Caspase activity, which mediated the proapoptotic action of Bcl-2, was determined on the basis of transformed ability of caspases 3, 8, and 9 (Roche Diagnostics GmbH, Mannheim, Germany). The increase in light absorbance at 405 nm was used to quantify the change of caspase activity. Then quantitative assessment of apoptotic HSCs was assessed by Hoechst 33258 (Beyotime Institute of Biotechnology, Jiangsu, China) staining and TUNEL method, which examined DNA strand breaks during apoptosis with One Step TUNEL Apoptosis Assay Kit (Oncor, Gaithersburg, USA) [17,18]. Flow cytometry was also performed to detect apoptosis by

Table 2
Primers used in TaqMan qRT-PCR.

Gene	Annealing temperature (°C)	Accession No.	Product size (bp)	Number gene primer (5′ → 3′)
U6	62	K00784	89	F:5′-GCTTCGGCAGCACATATACTAAAAT-3′ R:5′-CGCTTCACGAATTTGCGTGTCAT-3′
rno-mir-15b	62	MIMAT0000784	64	GSP:5′-GGGGTAGCAGCACATCATG-3′ R:5′-GTGCGTGTCGTGGAGTCG-3′
rno-mir-16	62	MIMAT0000785	64	GSP:5′-GGGGTAGCAGCACGTAAATA-3′ R:5′-GTGCGTGTCGTGGAGTCG-3′
rno-miR-122	60	MIMAT0000827	63	F:5′-GGGTGGAGTGTGACAATGG-3′ R:5′-GTGCGTGTCGTGGAGTCG-3′
rno-miR-143	60	MIMAT0000849	65	F:5′-GGGTGAGATGAAGCACTGT-3′ R:5′-CAGTGCGTGTCGTGGAGT-3′
rno-miR-138	60	MIMAT0000844	66	F:5′-GGGAGCTGGTGTTGTGAAT-3′ R:5′-CAGTGCGTGTCGTGGAGT-3′
rno-miR-140	60	MIMAT0000573	61	F:5′-GGCAGTGGTTTTACCCT-3′ R:5′-TGCGTGTCGTGGAGTC-3′

F, forward primer; R, reverse primer; GSP, gene specific primer. miRNA number and the sequence of a specific miRNA can be obtained from miRBase sequences (http://microrna.sanger.ac.uk).

Table 3
mature miRNAs duplexes.

Gene	Sense sequence	Antisense sequence
miRNA15b	5′-ACAUUUGGUACUACACGACGAU-3′	5′-CGUCGUGUAGUACCAAAUGUUU-3′
miRNA16	5′-UAGCAGCACGUAAAUAUUGGCG-3′	5′-CCAAUAUUUACGUGCUGCAAAU-3′
Negative control	5′-UUCUCCGAACGUGUCACGUTT-3′	5′-ACGUGACACGUUCGGAGAATT-3′

determining the relative amount of AnnexinV-FITC-positive-PI-negative cells (Bender MedSystems, Vienna, Austria), as previously described [19].

2.9. Statistical analysis

All the results were expressed as mean ± standard deviation (SD). Statistical analysis was done with Student's *t*-test for comparison of two groups, and ANOVA for multiple comparisons. In both cases, differences with $P < 0.05$ were considered statistically significant.

3. Results

3.1. In vitro activation of rat HSCs

About 5×10^8 ml^{-1} HSCs were harvested from each rat. The fraction of freshly isolated living HSCs was up to 95%, as defined by trypan blue staining. These cells were small and round with the quiescent phenotype at 48 h. When stimulated at 327 nm wavelength, up to

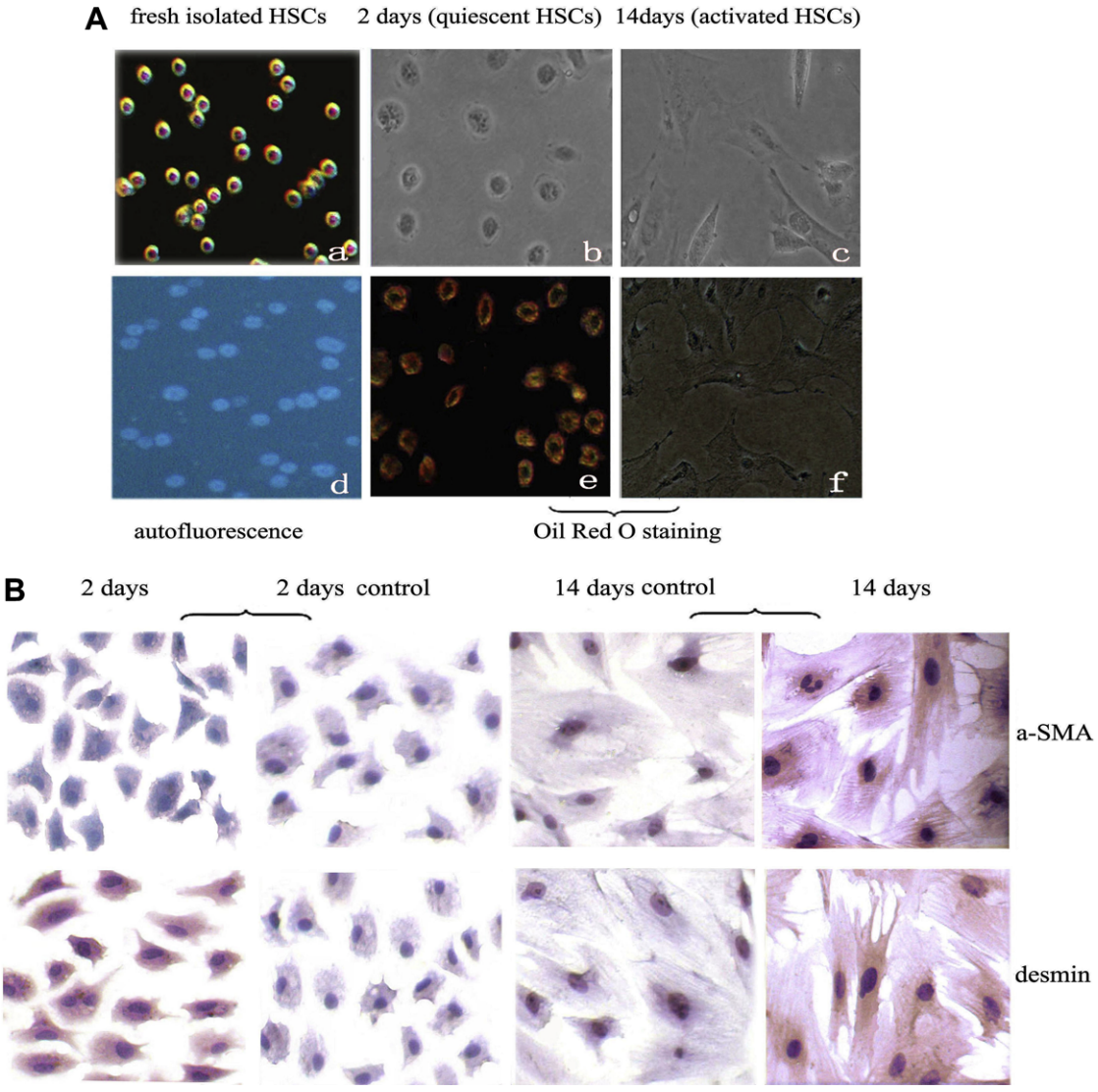

Fig. 1. (A) Characterization of HSCs isolated from rat liver (400×). (a) Cell morphology of isolated cultured HSC. (b, c) After isolation, the cells were cultured for 2 days (quiescent HSCs) or for 14 days (activated HSCs). (d) Spontaneous fluorescence of cultured HSCs at 24 h. (e, f) Oil Red O staining of quiescent and activated HSCs. (B) Immunocytochemistry staining of quiescent and activated HSCs for desmin and alpha-SMA. 266 × 256 mm (600 × 600 DPI). [This figure appears in colour on the web.]

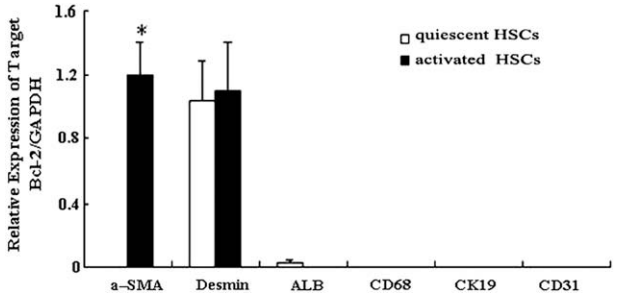

Fig. 2. QRT-PCR for desmin, alpha-SMA, ALB, CD31, CD68, and CK-19 demonstrate the purity of quiescent and activated HSCs. The purity of isolated HSCs is above 95%. Statistically significant difference between quiescent and activated HSCs is indicated by $^{*}P < 0.01$. 157 × 98 mm (600 × 600 DPI).

95% of HSCs had blue–green intrinsic autofluorescence due to the presence of vitamin A-rich oil droplets. Staining with Oil red O revealed that apparently intracellular lipid droplets existed only in quiescent HSCs.

Nevertheless, HSCs became highly activated after culture for 14 days. They presented a wall-adhesive growth pattern and many spindle-like or asteroid membranous processes without vitamin A droplets. Moreover, both immunocytochemical staining and qRT-PCR for α-SMA demonstrated the activated phenotype of HSCs (Figs. 1 and 2).

More than 95% of desmin-positive HSCs, together with absent expression of biomarkers specific for other liver cell populations, e.g. albumin (for hepatocytes), CD31 (for endothelial cells), CD68 (for Kupffer cells), and cytokeratin-19 (for cholangiocytes), further proved the purity of quiescent and activated HSCs at days 2 and 14 (Figs. 1 and 2).

3.2. miRNA expression profiles of quiescent and activated HSCs

Using the miRCURY LNA Array platform consisting of 384-well plates, we first assessed the miRNA expression profiles in quiescent and activated rat HSCs. The expression profiles of 279 miRNAs determined to be regulated between quiescent and activated rat HSCs were sufficient to separate samples into biologically interpretable groups. Among these, 12 miRNAs were identified to be upregulated more than 2-fold in activated HSCs as compared to that in quiescent HSCs, while nine miRNAs were less than the threshold level (0.5-fold) set during the progression of HSCs activation (Table 4) (Fig. 3A).

Six miRNAs among these filtered ones were validated to be significantly different between the activated and quiescent HSCs ($P < 0.05$). As shown in (Fig. 3B and C), the levels of miR-15b, miR-16, and miR-122 were

Table 4
The list of miRNAs identified in quiescent and activated rat hscs.

miRNA	Chromosomal location	14d hscs mean	2d hscs mean	Fold change	*P*-value	Function
Upregulated microRNAs						
rno-miR-874	17p14	1.953921	0.054115	36.106720	0.002530	
rno-miR-29c*	13q27	2.553848	0.102453	24.926960	0.001570	
rno-miR-501	Xq13	2.191427	0.100963	21.705330	6.08E-05	
rno-miR-349	7q34	2.247498	0.116357	19.315520	8.27E-05	
rno-miR-325-5p	Xq31	3.804137	0.210616	18.061930	0.013700	
rno-miR-328	19q11	2.816639	0.179430	15.697680	0.004080	
rno-miR-138	8q32	2.280723	0.191112	11.933970	0.000243	Apoptosis
rno-miR-143	18q12.1	2.575744	0.290671	8.861360	0.008340	Apoptosis
rno-miR-207	5q33	1.624586	0.316980	5.125201	0.005550	
rno-miR-872	5q33	1.909437	0.544651	3.505800	0.016100	
rno-miR-140	19q12	1.528697	0.724541	2.109884	0.042700	Apoptosis
rno-miR-193	10q25	1.409281	0.683853	2.060795	0.00194	Apoptosis
Downregulated microRNAs						
rno-miR-341	6q32	0.652910	1.353793	0.482282	0.011200	
rno-miR-20b-3p	Xq36	0.606460	1.313508	0.461710	0.035900	Proliferation
rno-miR-15	2q31	0.600000	1.598000	0.375469	0.000300	Apoptosis
rno-miR-16	2q31	0.598700	1.611884	0.371428	0.003400	Apoptosis
rno-miR-375	9q33	0.450975	1.657254	0.272122	0.000325	Signal transduction
rno-miR-122	18q12.1	0.416159	1.555468	0.267546	0.006320	Metabolism
rno-miR-146a	10q21	0.333576	1.515239	0.220147	0.014100	Proinflammation
rno-miR-92b	2q34	0.349742	1.699216	0.205825	0.017200	Cell growth
rno-miR-126	3p13	0.234475	1.786231	0.131268	0.003670	Cell growth

The list of miRNAs identified in quiescent and activated rat hscs with their mean expression values determined following global normalization and statistical analysis using student's *t*-test as described in the Section 2. Fold increase in activated HSCs compared to quiescent HSC experiments is shown (increased expression 2-fold). The *P*-values for activated vs quiescent HSCs for each gene are <0.05.
Fold decrease in activated HSCs compared to quiescent HSC experiments is shown (Decreased expression 0.5-fold). The *P*-values for activated vs quiescent HSCs for each gene are <0.05.

downregulated in activated HSCs rather than quiescent ones, while the miR-138, miR-143, and miR-140 showed an opposite expression pattern, in agreement with the results of microarray hybridyzation.

3.3. Microarray-based GO analysis revealed the role of miR-15b and miR-16 in activated HSCs

According to the threshold of GOs significant regulated by miRNAs, the *P*-value and *FDR* was <0.001 and <0.05, respectively. The high-enrichment GOs targeted by over-expressed miRNAs were potassium ion transport, positive regulation of transcription from RNA polymerase II promoter, cell proliferation, etc. In contrast, significant GOs corresponding to under-expressed miRNAs appeared to be apoptosis, lipid metabolic process, DNA repair, etc. Among these, the maximum-enriched-GO relating to apoptosis, together with the plentiful miRNAs interacted with apoptosis-related genes, suggested them an important role in the activation of HSCs (Fig. 4).

The miRNA–mRNA regulatory networks based on apoptosis-related GO, being established in Fig. 5, distinguished the putative target mRNAs between over-expressed and under-expressed miRNAs. Four over-expressed miRNAs (miR-140, miR-207, miR-325-5p, and miR-874) showed the most target mRNAs of 7 (degree 7). However, miR-16, which had the highest degree of 5 in under-expressed miRNAs, and miR-15b regulated some important genes, including the antiapoptotic gene of Bcl-2. miR-15/16 family and Bcl-2, therefore, might be of great importance to the activation of HSCs.

3.4. miR-15b and miR-16 downregulated Bcl-2 at the posttranscriptional level

Examination of the homology between miR-15b/16 and Bcl-2 mRNA sequences showed that the six nucleotides in the seed region of miR-15b/16 were complementary to bases 892–897 of Bcl-2 3′UTR (NM_016993). Thus an inhibitory effect of miR-15b and miR-16 on Bcl-2 was inferred.

To further investigate the actions of miR-15b and miR-16 on Bcl-2, the expression of Bcl-2 was investigated at the mRNA and protein levels. Both RT-PCR and Western

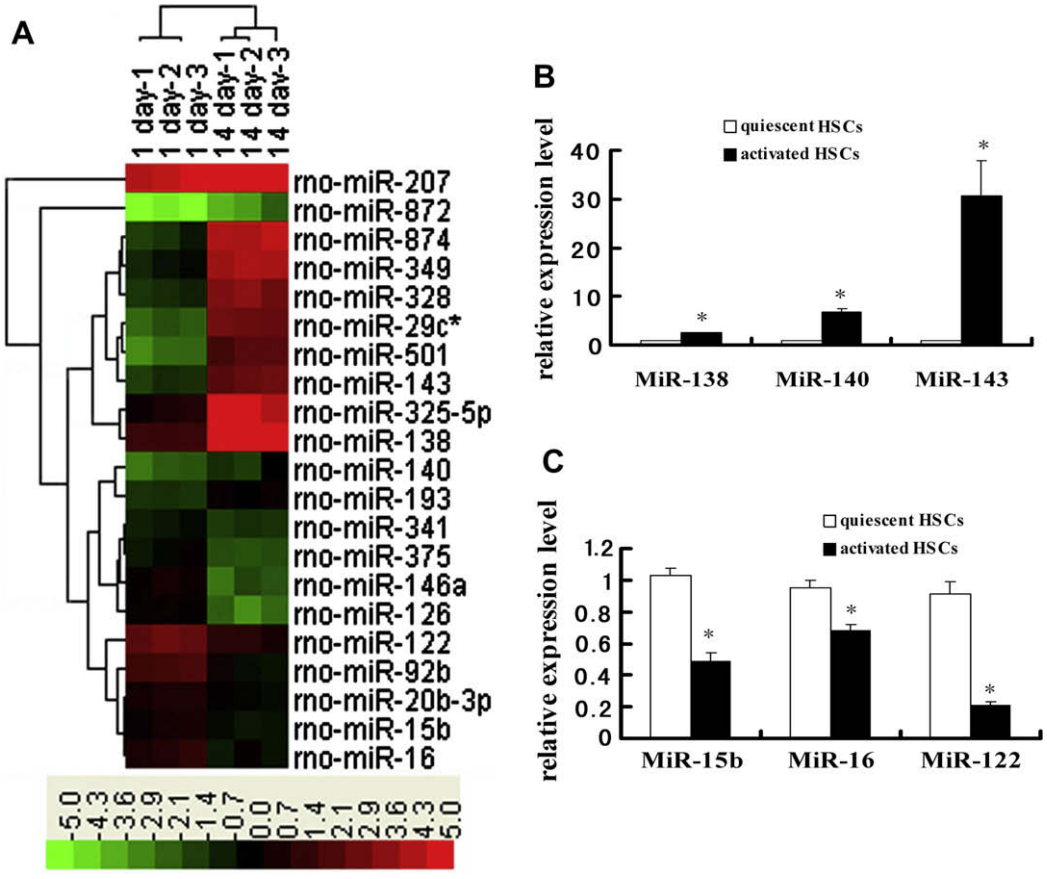

Fig. 3. (A) miRNA profiles differentiate activated HSCs (14 days) from quiescent HSCs (2 days). Samples consist of paired samples from three rats. Both down-regulated (green) and up-regulated (red) miRNAs were identified in HSCs. (B, C) Validation of microarray data using real-time RT-PCR. Triplicate assays were done for each RNA sample and the relative amount of each miRNA was normalized to U6 snRNA. Statistically significant difference between quiescent and activated HSCs is indicated by $^{*}P < 0.01$. 264 × 186 mm (600 × 600 DPI). (For interpretation of the references to color in this figure legend, the reader is referred to the web version of this paper.) [This figure appears in colour on the web.]

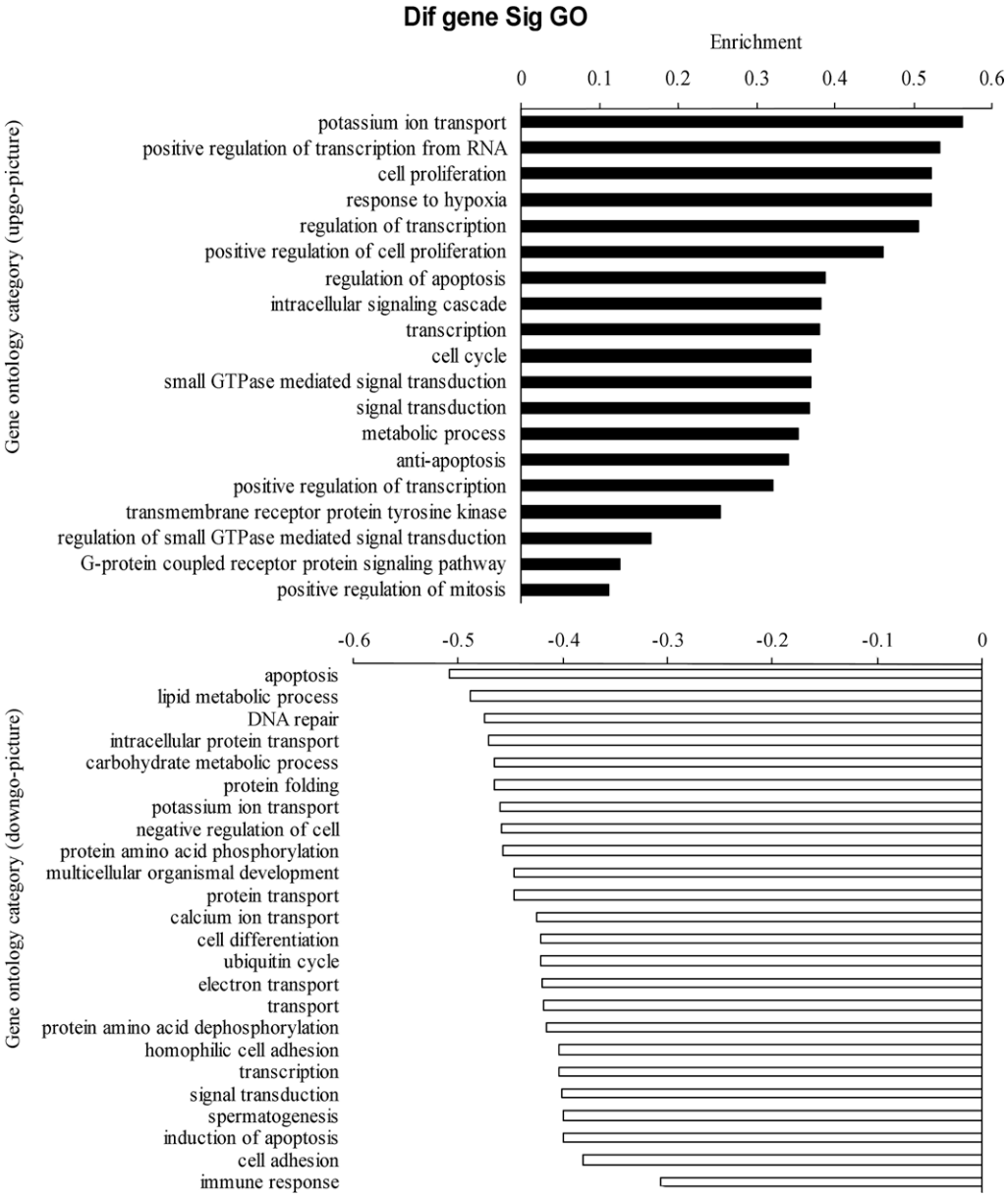

Fig. 4. microRNA target significant G. The upper chart composes the GOs targeted by overexpressed miRNA, and the lower chart composes the GOs targeted by down-expressed miRNA. All these GOs show increased enrichment. The vertical axis is the GO category and the horizontal axis is the enrichment of GO. 197 × 235 mm (400 × 400 DPI).

blot analysis exhibited obviously increased level of Bcl-2 in activated HSCs when compared to that in quiescent ones ($P < 0.05$). Although there was no significant difference in Bcl-2 mRNA, transfection of miR-15b or miR-16 for 24 h induced the prominent reduction of Bcl-2 at the posttranslational level. Moreover, the inhibition of Bcl-2 expression was observed to be paralleled with the miRNA concentration. The efficacy of miRNAs, however, kept constantly above 100 nM (Fig. 6).

Being assessed by the dual luciferase assay, significant decrease in relative luciferase activity was noted when pGL3-Bcl2-3′UTR was cotransfected with miR-15b or miR-16 mimics. As expected, this suppressive effect could be abolished by partially deleting the perfectly complementary sequences in the 3′-UTR of Bcl-2 mRNA (pGL3-mutBcl-2-3′-UTR), which disrupted the interaction between miR-15b/miR-16 and Bcl-2 (Fig. 7). These demonstrations confirmed the direct interaction of both miRNAs and Bcl-2.

3.5. Bcl-2 inhibition by miR-15b and miR-16 induced apoptosis of activated HSCs

According to the morphologic observation, the shape of activated HSCs treated by miR-15b or miR-16 remodeled from stellate or shuttle to spherical, and the

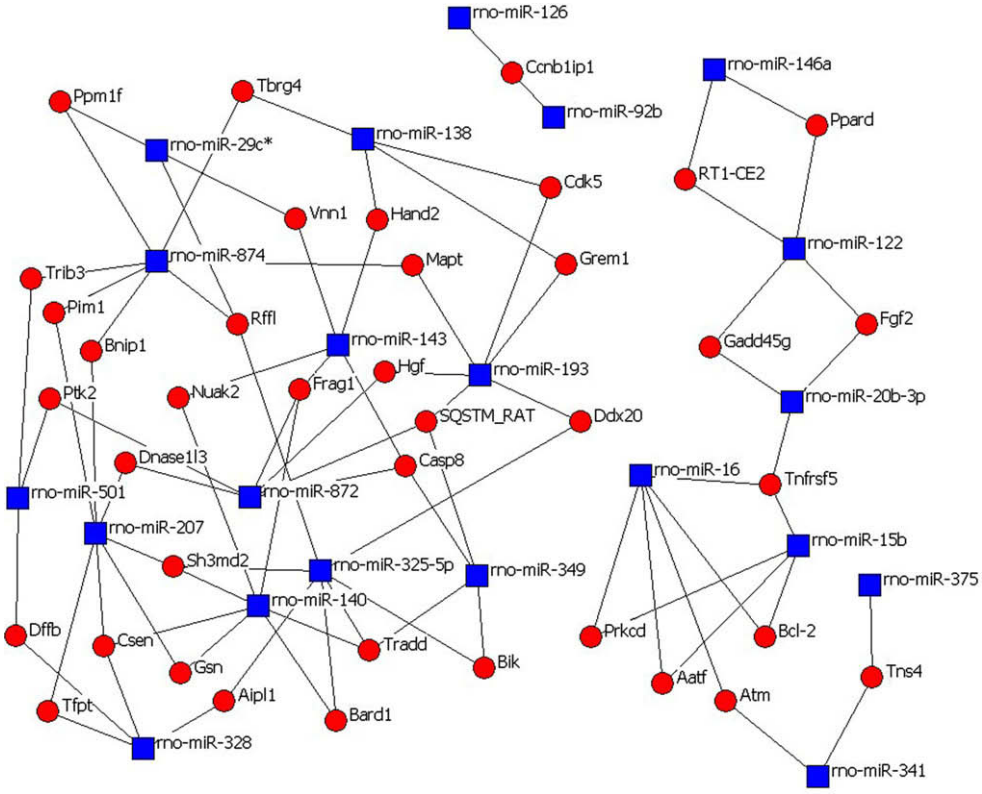

Fig. 5. microRNA-gene-network. Blue box nodes represent microRNA, and red cycle nodes represent mRNA. Edges describe the inhibitive effect of microRNA on mRNA. The left is the over-expression microRNA-mRNA network, and the right is the under-expression microRNA-mRNA network. 211 × 172 mm (600 × 600 DPI). [This figure appears in colour on the web.]

intercellular space was enlarged. The cell detached from the plate could be detected at 12 h, and was more noticeable at 24 h (Fig. 8A).

To confirm apoptosis at the single-cell level, the Hoechst 33258 staining, TUNEL staining, and annexin-V/PI assay were employed. Fluorescence microscopy of HSCs showed typical apoptotic morphological changes, such as condensed chromatin and shrunken nuclei by Hoechst 33258 staining, and yellowish green apoptotic cells by TUNEL staining (Fig. 8B–D). Exposure to 50–100 nM miR-15b or miR-16 also increased the rate of apoptosis in a concentration-dependent manner, then plateaued at higher concentrations (Fig. 9A) (Table 5). As compared to that of control, the enzymatic activities of caspases 3, 8, and 9, the key executioners of apoptosis, increased significantly at the concentration of 100 nM miR-15b or miR-16. But there was no significantly different activity of these enzymes between miR-15b and miR-16 treated HSCs (Fig. 9B).

4. Discussion

HSCs, the major mesenchymal cells of liver, act as the inducer of liver fibrosis after their transdifferentiation into myofibroblast-like cells [20]. This process of activation is accompanied by a series of pathological changes on the basis of large-scale gene over-expression and/or under-expression [4]. However, limited understanding of the gene regulation made the HSC activation still vague and controversial until now.

Increasing evidence has confirmed miRNA to be one of the most important, even pivotal, factors controlling gene expression. Therefore, we evaluated the miRNA expression profile during the activation of rat HSCs. Being compared to that of quiescent HSCs, microarray revealed a set of differentially expressed miRNAs, with 12 significantly upregulated and nine significantly down-regulated miRNAs in activated HSCs. Tests of miR-16, miR-15b, miR-122, miR-138, miR-143, miR-140 further validated the reliability of micoarray hybridization.

In addition, GO enrichment analysis, which was based on the reported and predicted target genes of these miRNAs, had been developed to shed light on whether particular functions were enriched among genes controlling distinctive characters between reference group and test group. GO organized genes targeted by differential miRNAs into hierarchical categories based on biological process, and then outlined the effects of miRNAs on HSC activation through abundant high-enrichment GOs. Initially, resting HSCs were stimulated by fibrosis-related cytokines through a G protein-coupled receptor protein

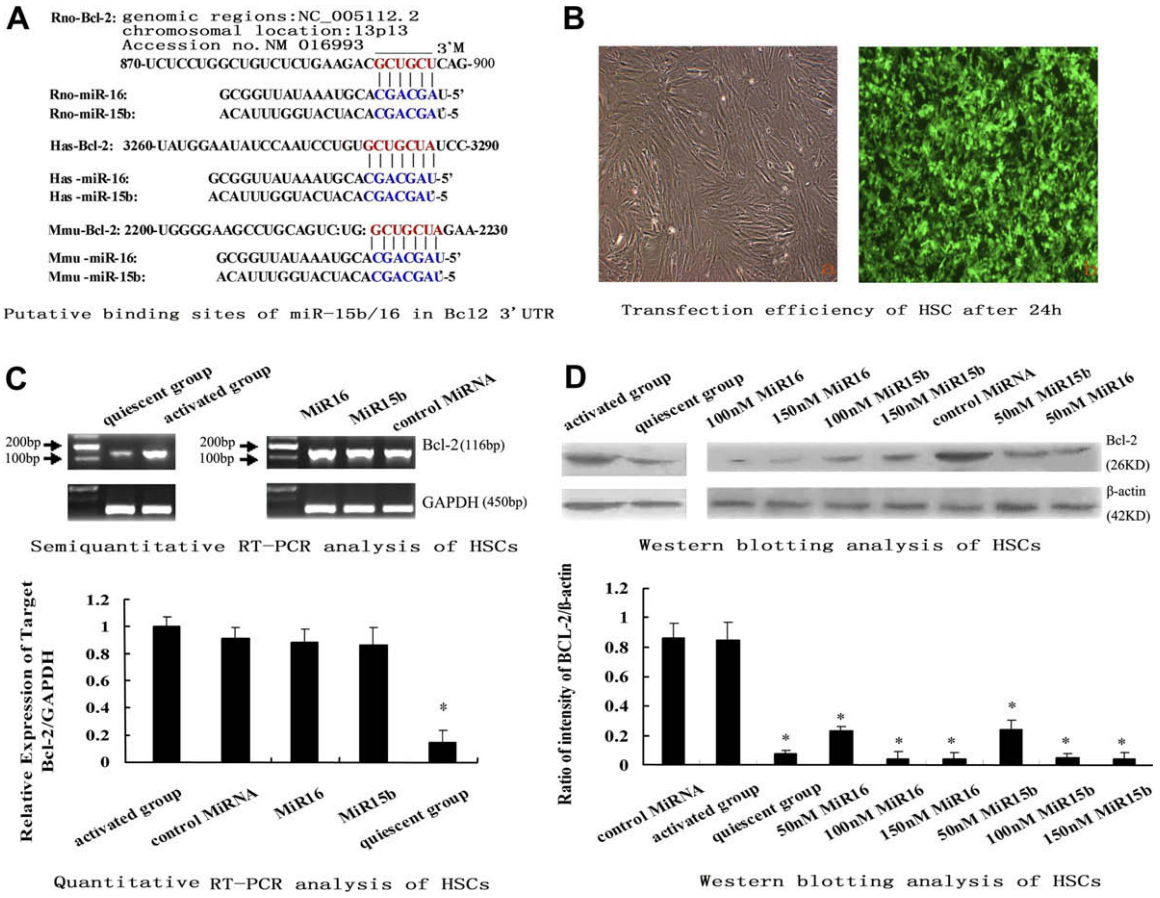

Fig. 6. Bcl-2 is the target of miR-15b and miR-16. A miR-15b and miR-16 share the conserved binding sites in Bcl-2 3′UTR (rat, human and mouse). The site of target mutagenesis is indicated (3′M). B Transfection efficiency of HSCs after 24 h (200×) (A) light microscope of HSC transfected with fluorescently labeled miRNA after 24 h. (B) fluorescence microscope of HSC transfected with fluorescently labeled miRNA after 24 h. (C) The mRNA levels of Bcl-2 in quiescent and activated HSCs as detected by Semiquantitative RT-PCR and analyzed by quantitative real-time PCR. (D) The protein levels of Bcl-2 in quiescent and activated HSCs detected by Western blotting. $^{*}P < 0.01$ versus corresponding control using Student's *t*-test. 289 × 223 mm (500 × 500 DPI). [This figure appears in colour on the web.]

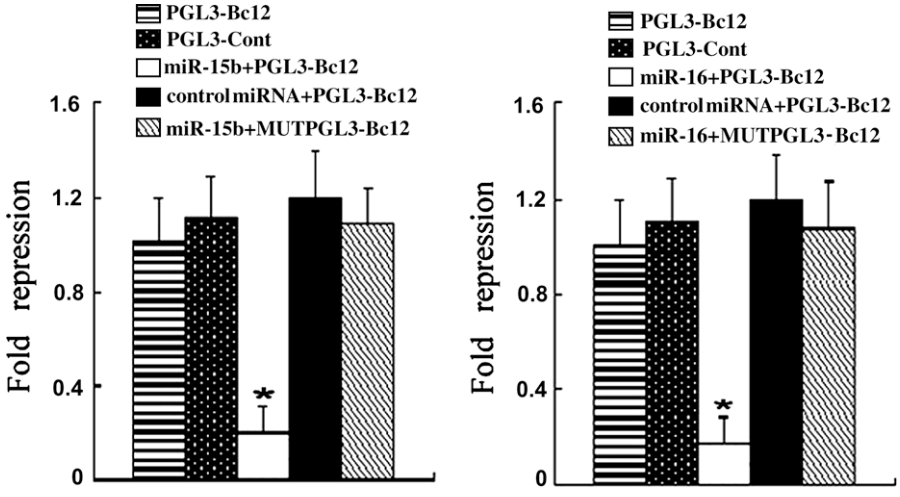

Fig. 7. Dual luciferase assay is performed in activated HSCs, which has been transfected with luciferase construct alone or cotransfected with miR-15b or miR-16 mimics or mimics control. Firefly luciferase construct containing mutant (MutPGL3-Bcl2) target site of the Bcl-2 3′UTR is generated and transfected as indicated. Firefly luciferase activity is normalized to Renilla luciferase activity for each sample. $^{*}P < 0.01$ compared to pGL3-BCL-2. 108 × 33 mm (600 × 600 DPI).

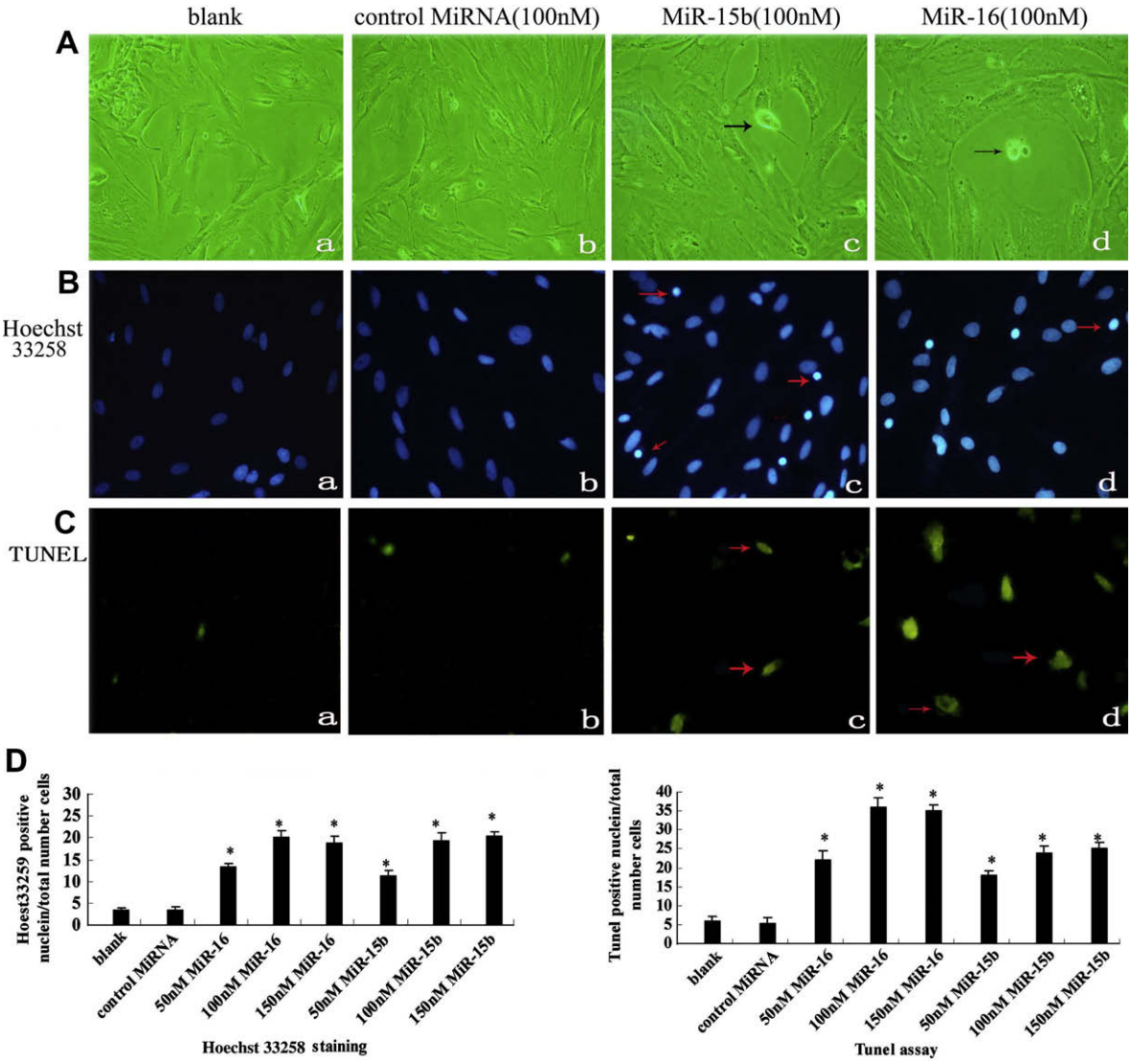

Fig. 8. The effects of miR-15b and miR-16 on apoptosis of activated HSCs. (A) Light microscope of HSCs (×400) (a) Blank (without miRNA); (b) 100 nM control miRNA; (c) 100 nM miR-15b; (d) 100 nM miR-16. (B, C) Fluorescent images of HSCs using Hoechst 33258 staining and TUNEL assay (400×) (a) blank (without miRNA); (b) 100 nM control miRNA; (c) 100 nM miR-15b; (d) 100 nM miR-16. (D) Analysis of Hoechst 33258 staining and TUNEL assay. Apoptotic rate is determined by comparing the number of apoptotic cells to the total cells. Statistically significant difference between control and miRNAs is indicated by $P < 0.01$. 300 × 277 mm (500 × 500 DPI). [This figure appears in colour on the web.]

signaling pathway. Activation-inducing signals were then transducted by transmembrane tyrosine kinases, small GTPase-mediated signal transduction and an intracellular signaling cascade. Thereafter, various phenotypes of HSCs, including proliferation, apoptosis, cell cycle, differentiation, carbohydrate and lipid metabolism, intercellular adhesion etc., altered on the basis of protein amino acid phosphorylation/dephosphorylation and transcriptional regulation.

In contrast to mitogenesis and differentiation, GOs concerning apoptosis seemed to dominate the significant GO categories. A key role of miRNAs in the apoptosis of HSCs was suggested. miRNA–gene interaction networks based on apoptosis-related GOs further displayed some critical members of the mitochondrial apoptosis pathway; i.e., Bcl-2 and Bim of the Bcl-2 family, and the regulatory miRNA (miR-15b, miR-16) of Bcl-2. Integrated bioinformation analysis of differentially expressed miRNAs verified that miR-15b and miR-16, members of the miR-15/16 family, were the only miRNAs targeting Bcl-2 with 6 complementary nucleotides. Bcl-2, which can be rarely detected in the normal HSCs and non-proliferative senescent HSCs, is expressed in culture-activated HSCs and intra-hepatic HSCs after CCl_4 injury [21,22]. Recent studies have attributed the apoptosis-resistance of HSCs to the over-expression of Bcl-2 [23]. Taken together, miR-15b and miR-16 are likely to participate in apoptosis of HSCs by targeting Bcl-2 and the downstream protease cascade.

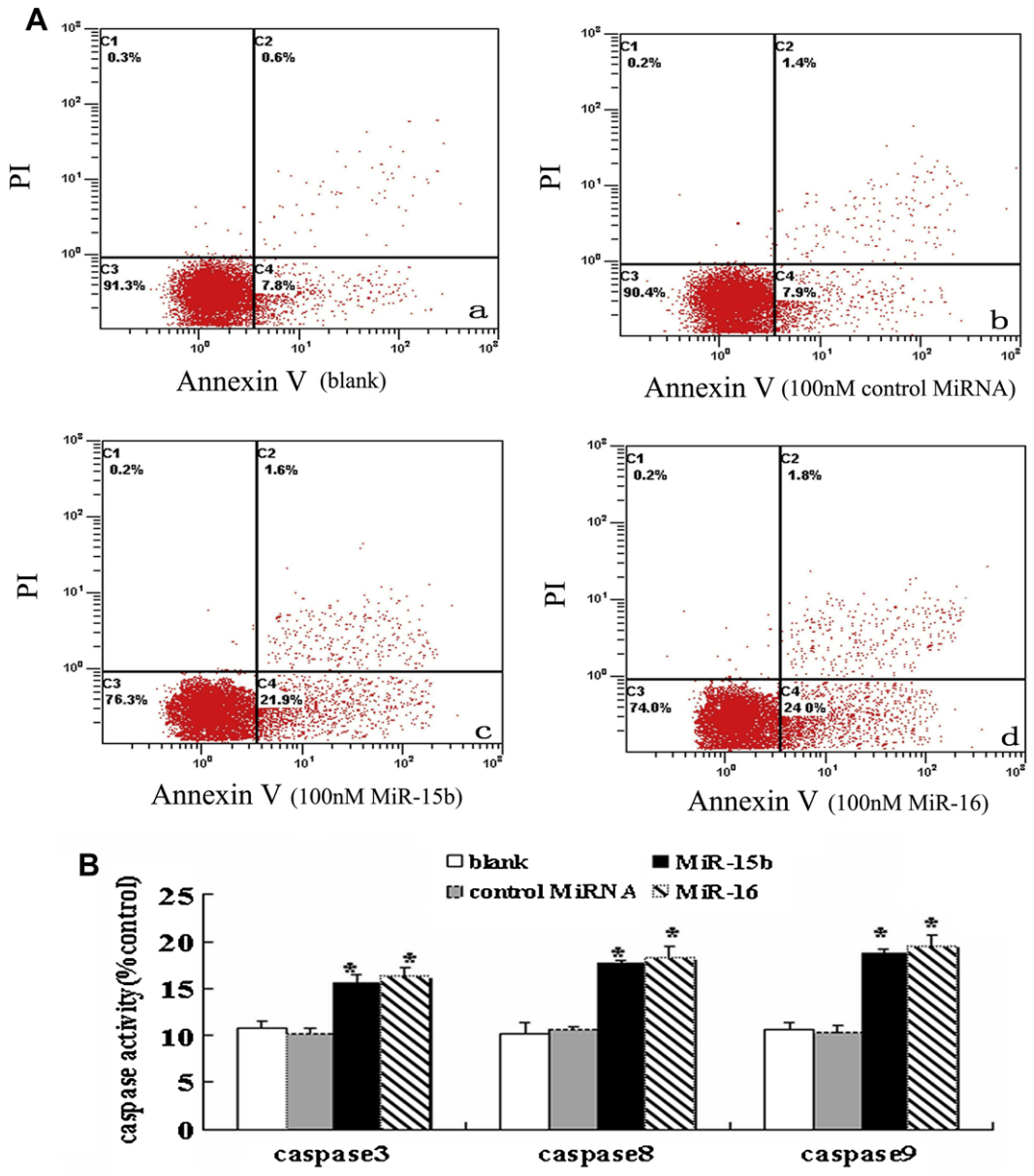

Fig. 9. (A) Annexin-V/PI combined labeling flow cytometry. (a) Blank (without miRNA); (b)100 nM control miRNA; (c) 100 nM miR-15b; (d) 100 nM miR-16. (B) Activity of caspases 3, 8, and 9 is assessed at 24 h after transfection with miR-15b mimic, miR-16 mimics, or the miRNA mimic control in activated HSCs. Statistically significant difference between control and other groups is indicated by $P < 0.01$. 255 × 284 mm 600 × 600 DPI). [This figure appears in colour on the web.]

Our experimental findings were consistent with these reports that a large amount of Bcl-2 could be detected at the protein and mRNA levels in activated instead of quiescent HSCs [23,24]. Moreover, the levels of miR-15b and miR-16 were inversely correlated with that of Bcl-2 in both quiescent and activated HSCs, which was also

Table 5
Annexin-V/PI labeling to detect apoptotic rate.

	Blank	Control MiRNAs	Mir-16 (50 nM)	Mir-16 (100 nM)	Mir-16 (150 nM)	Mir-15 (50 nM)	Mir-15 (100 nM)	Mir-15 (150 nM)	*P*-value
Survived cells	91.3 ± 1.1	90.4 ± 0.8	84.3 ± 2.1	74.0 ± 1.8	64.8 ± 0.8	86.3 ± 2.1	75.4 ± 1.8	63.8 ± 1.8	
Apoptotic cells	7.8 ± 1.2	7.9 ± 1.0	14.3 ± 0.3*	24.6 ± 1.5*	26.1 ± 2.0*	12.3 ± 0.3*	23.3 ± 1.5*	24.1 ± 1.0*	$P < 0.05$
Necrotic cells	0.5 ± 0.1	1.7 ± 0.3	1.5 ± 0.2	1.8 ± 0.3	8.9 ± 0.5*,#	1.4 ± 0.2	1.8 ± 0.5	9.0 ± 0.1*,#	$P =$ NS

Apoptotic evaluation determined through comparison of apoptotic cell and total number of cells. NS, not significant.
* Indicates *P*-values < 0.05 between control and miRNAs.
# Indicates *P*-values < 0.01 between blank and miRNAs.

in agreement with earlier studies [25,26]. Similarly, transfection of mir-15b or miR-16 greatly reduced Bcl-2, but not Bcl-2 mRNA, and the luciferase activity of Bcl-2 3′UTR-based reporter construct in HSCs. Thus Bcl-2 was indicated to be a direct target of miR-15b and miR-16. As a result, proteases downstream of Bcl-2 (caspases 3, 8, and 9) activated greatly, which reflected the activation of caspase signaling pathway and the irreversible phase of apoptosis. A combination of Hoest 33258 staining, TUNEL and flow cytometry also demonstrated prominent apoptosis in miR-15b-treated or miR-16-treated activated HSCs. This phenomenon provided substantial evidence for the first time that restoration of the level of either miR-15b or miR-16 was sufficient to induce the apoptotic process in HSCs with myofibroblast-like phenotype. In addition, the most evident pro-apoptosis effect was observed in the group treated with a medium dose of miRNA (100 nM) in both the miR-15b-treated and miR-16-treated groups.

Apart from Bcl-2-induced apoptosis, there are other signaling pathways relevant to HSCs apoptosis, especially the Fas/FasL-mediated pathway [27]. Nevertheless, critical members of Fas/FasL signaling or Fas/FasL-related miRNAs were not found within the apoptosis-related GOs or miRNA–gene networks. However, unexplored miRNAs other than miR-15b and miR-16 may be involved in the process.

In conclusion, the activation of cultured rat HSCs is related to 21 miRNAs. Their wide range of actions may regulate multiple functions, especially apoptosis of HSCs. Both miR-15b and miR-16, which characterize the miRNA–gene regulatory networks, are probably essential for apoptosis by targeting Bcl-2 and the caspase signaling cascade. These findings may not only highlight the essence of HSCs activation, but also facilitate our access to novel therapeutic strategy against fibrosis and offer insight into its progression.

Acknowledgements

This work is supported by the Foundation of Shanghai Commission of Science Technology of Research Program (O7JC14044). Genminix company provides us with technical assistance.

References

[1] Aleffi S, Petrai I, Bertolani C, Parola M, Colombatto S, Novo E, et al. Upregulation of proinflammatory and proangiogenic cytokines by leptin in human hepatic stellate cells. Hepatology 2005;42:1339–1348.
[2] Friedman SL. Mechanisms of disease: mechanisms of hepatic fibrosis and therapeutic implications. Nat Clin Pract Gastroenterol Hepatol 2004;1:98–105.
[3] Kruglov EA, Correa PR, Arora G, Yu J, Nathanson MH, Dranoff JA. Molecular basis for calcium signaling in hepatic stellate cells. Am J Physiol Gastrointest Liver Physiol 2007;292:975–982.
[4] Jiang F, Parsons CJ, Stefanovic B. Gene expression profile of quiescent and activated rat hepatic stellate cells implicates Wnt signaling pathway in activation. J Hepatol 2006;45:401–409.
[5] Chitwood DH, Timmermans MC. Target mimics modulate miRNAs. Nat Genet 2007;39:935–936.
[6] Ambros V. The functions of animal microRNAs. Nature 2004;431:350–355.
[7] Chen CZ, Li L, Lodish HF, Bartel DP. MicroRNAs modulate hematopoietic lineage differentiation. Science 2004;303:83–86.
[8] Roldo C, Missiaglia E, Hagan JP, Falconi M, Capelli P, Bersani S, et al. MicroRNA expression abnormalities in pancreatic endocrine and acinar tumors are associated with distinctive pathologic features and clinical behavior. J Clin Oncol 2006;24:4677–4684.
[9] Zhao JJ, Hua YJ, Sun DG, Meng XX, Xiao HS, Ma X. Genome-wide microRNA profiling in human fetal nervous tissues by oligonucleotide microarray. Childs Nerv Syst 2006;22:1419–1425.
[10] Friedman SL, Roll FJ. Isolation and culture of hepatic lipocytes, Kupffer cells, and sinusoidal endothelial cells by density gradient centrifugation with Stractan. Anal Biochem 1987;161:207–218.
[11] Ying-Bin Hu, Ding-Guo Li, Han-Ming Lu. Modified synthetic siRNA targeting tissue inhibitor of metalloproteinase-2 inhibits hepatic fibrogenesis in rats. J Gene Med 2007;9:217–229.
[12] Cassiman D, Denef C, Desmet V, Roskams T. Human and rat hepatic stellate cells express neurotrophins and neurotrophin receptors. Hepatology 2001;33:148–158.
[13] Chen C, Ridzon DA, Broomer AJ, Zhou Z, Lee DH, Nguyen JT, et al. Real-time quantification of microRNAs by stem-loop RT-PCR. Nucleic Acids Res 2005;33:e179.
[14] Livak KJ, Schmittgen TD. Analysis of relative gene expression data using real-time quantitative PCR and the 2(-Delta Delta C(T))method. Methods 2001;25:402–408.
[15] Gene Ontology Consortium. The Gene Ontology (GO) project in 2006. Nucleic Acids Res 2006;34:322-326.
[16] Lim LP, Lau NC, Garrett-Engele P, Grimson A, Schelter JM, Castle J, et al. Microarray analysis shows that some microRNAs downregulate large numbers of target mRNAs. Nature 2005;433:769–773.
[17] Jiang P, Yan PK, Chen JX, Zhu BY, Lei XY, Yin WD. High density lipoprotein 3 inhibits oxidized low density lipoproteininduced apoptosis via promoting cholesterol efflux in RAW264.7 cells. Acta Pharmacologica Sinica 2006;27:151–157.
[18] Gold R, Schmied M, Giegerich G, Breitschopf H, Hartung HP, Toyka KV. Differentiation between cellular apoptosis and necrosis by the combined use of in situ tailing and nick translation techniques. Lab Invest 1994;71:219–225.
[19] Boersma AW, Nooter K, Oostrum RG, Stoter G. Quantification of apoptotic cells with fluorescein isothiocyanate-labeled annexin V in chinese hamster ovary cell cultures treated with cisplatin. Cytometry 1996;24:123–130.
[20] Inagaki Y, Kushida M, Higashi K, Itoh J, Higashiyama R, Hong YY, et al. Cell type-specific intervention of transforming growth factor beta/Smad signaling suppresses collagen gene expression and hepatic fibrosis in mice. Gastroenterology 2005;129:259–268.
[21] Lee JI, Lee KS, Paik YH, Nyun Park Y, Han KH, Chon CY, et al. Apoptosis of hepatic stellate cells in carbon tetrachloride induced acute liver injury of the rat: analysis of isolated hepatic stellate cells. J Hepatol 2003;39:960–966.
[22] Schnabl B, Purbeck CA, Choi YH, Hagedorn CH, Brenner D. Replicative senescence of activated human hepatic stellate cells is accompanied by a pronounced inflammatory but less fibrogenic phenotype. Hepatology 2003;37:653–664.
[23] Novo E, Marra F, Zamara E, Valfrè di Bonzo L, Monitillo L, Cannito S, et al. Overexpression of Bcl-2 by activated human hepatic stellate cells: resistance to apoptosis as a mechanism of progressive hepatic fibrogenesis in humans. Gut 2006;55:1174–1182.

[24] Kawada N. Human hepatic stellate cells are resistant to apoptosis: implications for human fibrogenic liver disease. Gut 2006;55: 1073–1074.
[25] Cimmino A, Calin GA, Fabbri M, Iorio MV, Ferracin M, Shimizu M. miR-15 and miR-16 induce apoptosis by targeting BCL2. Proc Natl Acad Sci USA 2005;102:13944–13949.
[26] Xia L, Zhang D, Du R, Pan Y, Zhao L, Sun S, et al. miR-15b and miR-16 modulate multidrug resistance by targeting BCL2 in human gastric cancer cells. Int J Cancer 2008;123:372–379.
[27] Wang XZ, Zhang SJ, Chen YX, Chen ZX, Huang YH, Zhang LJ. Effects of platelet-derived growth factor and interleukin-10 on Fas/Fas-ligand and Bcl-2/Bax mRNA expression in rat hepatic stellate cells in vitro. World J Gastroenterol 2004;10: 2706–2710.